Accepted for Publication in ApJ
Preprint typeset using LaTeX style emulateapj v. 6/22/04

MASS ALONG THE LINE OF SIGHT TO THE GRAVITATIONAL LENS B1608+656: GALAXY GROUPS AND IMPLICATIONS FOR H_0 *

C. D. Fassnacht, R. R. Gal, L. M. Lubin, J. P. McKean
Department of Physics, University of California, 1 Shields Avenue, Davis, CA 95616

Gordon K. Squires
Spitzer Science Center, California Institute of Technology, Mail Code 220-6, 1200 E. California Blvd., Pasadena, CA 91125

and

A. C. S. Readhead
Astronomy Department, 105-24, Caltech, Pasadena, CA 91125
Accepted for Publication in ApJ

ABSTRACT

We report the discovery of four groups of galaxies along the line of sight to the B1608+656 gravitational lens system. One group is at the redshift of the primary lensing galaxy ($z = 0.631$) and appears to have a low mass, with eight spectroscopically-confirmed members and an estimated velocity dispersion of 150±60 km s^{-1}. The three other groups are in the foreground of the lens. These groups contain ∼10 confirmed members each, and are located at redshifts of 0.265, 0.426, and 0.520. Two of the three additional groups are centered roughly on the lens system, while the third is centered $\sim 1'$ south of the lens. We investigate the effect of each of the four groups on the gravitational lensing potential of the B1608+656 system, with a particular focus on the implications for the value of H_0 derived from this system. We find that each group provides an external convergence (κ_{ext}) of ∼0.005–0.060, depending on the assumptions made in calculating the convergence. For lens systems where no additional observables that can break the mass-sheet degeneracy exist, the determination of H_0 will be biased high by a factor of $(1 - \kappa_{ext})^{-1}$ if the external convergence is not properly included in the model. For the B1608+656 system, the stellar velocity dispersion of the lensing galaxy has been measured, thus breaking the mass-sheet degeneracy due to the group that is physically associated with the lens. The effect of the other groups along the line of sight can be folded into the overall uncertainties due to large-scale structure (LSS) along the line of sight. Because the B1608+656 system appears to lie along an overdense line of sight, the LSS will cause the measurement of H_0 to be biased high for this system. The systematic bias introduced by LSS could be 5% or greater. Because LSS bias should be random along random lines of sight, averaging a large number of determinations of H_0 from different lens systems should substantially reduce the uncertainties due to LSS on the global lens-based measurement of H_0.

Subject headings: distance scale — galaxies: individual (CLASS B1608+656) — gravitational lensing – galaxies: groups

1. INTRODUCTION

One of the many possible uses of gravitational lens systems is the measurement of H_0 (Refsdal 1964). However, this method has been limited by a lack of knowledge about the mass distribution in the lens, which leads to degeneracies between model parameters and H_0. Perhaps the most important degeneracy is that between the radial slope of the lensing mass profile and H_0. However, strong limits can be placed on the mass slope in systems in which measurements of stellar velocity dispersions can be made (e.g., Treu & Koopmans 2004), more than one component of the source is multiply-imaged (e.g., Cohn et al. 2001), an Einstein ring is seen (e.g., Kochanek et al. 2001), or VLBI structure in the lensed images can be clearly mapped from one image to another (e.g., Rusin et al. 2002). Another major degeneracy is that caused by an extended mass distribution that is associated with the lens. This is the famous "mass-sheet degeneracy" (e.g., Falco et al. 1985) and can be caused by a cluster or group along the line of sight to the main lensing galaxy. The problem is that the standard lens observables, namely the locations and fluxes of the lensed images and the location of the lensing galaxy, do not indicate how much of the lensing mass surface density is due to the mass sheet. In fact, with the exception of very large separation lenses (e.g., SDSS J1004+4112 and Q0957+561; Oguri et al. 2004; Walsh, Carswell, & Weymann 1979), it is difficult to know from the standard lensing observables whether or not there even exists an associated group or cluster. Thus, it is necessary to search for such structures by other means. We are conducting a survey of lenses in which time delays have been measured, with the aim of detecting groups or clusters which can affect the determination of H_0 from those systems.

*BASED IN PART ON OBSERVATIONS MADE WITH THE NASA/ESA HUBBLE SPACE TELESCOPE, OBTAINED AT THE SPACE TELESCOPE SCIENCE INSTITUTE, WHICH IS OPERATED BY THE ASSOCIATION OF UNIVERSITIES FOR RESEARCH IN ASTRONOMY, INC., UNDER NASA CONTRACT NAS 5-26555. THESE OBSERVATIONS ARE ASSOCIATED WITH PROGRAM #GO-10158.
Electronic address: fassnacht@physics.ucdavis.edu

The CLASS B1608+656 system (Myers et al. 1995) is an excellent target for our survey. The redshifts of the lens and background source have been measured to be $z = 0.630$ and $z = 1.39$, respectively (Myers et al. 1995; Fassnacht et al. 1996). It remains the only four-image lens system for which robust and high-precision measurements of all three independent time delays have been made (Fassnacht et al. 2002). The lens has been subjected to intensive modeling, which incorporated information from the measured stellar velocity distribution and the Einstein ring shape. With an advanced modeling code, strong limits were placed on the slope of the mass density profile, yielding a measurement of $H_0 = 75^{+7}_{-6}$ km s^{-1} Mpc^{-1} (Koopmans et al. 2003). Furthermore, the mass models for this system require a relatively large external shear of nearly 0.1 (Koopmans et al. 2003), indicating the presence of nearby mass. In this paper, we provide evidence for a group of galaxies associated with the primary lensing galaxy and discuss the result that it and other structures along the line of sight have on the determination of H_0 from this system.

Throughout this paper we assume $\Omega_M = 0.3$, $\Omega_\Lambda = 0.7$, and, unless otherwise stated, we will express the Hubble Constant as $H_0 = 100h$ km s^{-1} Mpc^{-1}.

2. OBSERVATIONS AND DATA REDUCTION

We have conducted a spectroscopic survey of the B1608+656 field as part of our ongoing program to find compact groups of galaxies associated with gravitational lenses. The field was imaged in three bands, Gunn g, r, and i (Thuan & Gunn 1976), with the Palomar 60-Inch Telescope. Spectroscopic targets were selected based on their colors and distances from the lens system. The highest priority targets were those close to the lens system and with $(r - i)$ colors in the range 0.45 to 0.65, i.e., close to those expected for early-type galaxies at the redshift of the lensing galaxy. All of the spectroscopic targets had $r \leq 23$. In addition to the high priority targets, several other galaxies were observed in order to pack efficiently the slitmasks that were used for the bulk of the spectroscopy. The spectroscopic observations were made with the Low Resolution Imaging Spectrograph (LRIS; Oke et al. 1995), in both longslit and multislit modes, and the Echellete Spectrograph and Imager (ESI; Sheinis et al. 2002) on the W. M. Keck Telescopes. The spectroscopic data were reduced using scripts based on standard IRAF[1] tasks. Additional IDL scripts were used to process the ESI data. The spectroscopic and photometric data on all of the surveyed galaxies, along with the full details of the data reduction procedures, will be presented in a future paper dealing with the properties of the groups and the galaxies within them.

3. MASS ALONG THE LINE OF SIGHT TO B1608+656

The spectroscopic observations produced redshifts for 97 galaxies in the field. The typical uncertainties in the redshifts, based on the scatter of redshifts calculated from individual lines in each spectrum, were $\sigma_z \sim 0.0003$. The distribution of redshifts, in which several spikes are seen, is shown in Figure 1. We select group or cluster candidates by looking for structures that are concentrated both spatially and in redshift space, using the iterative method described by Wilman et al. (2005). We investigated structures with at least five members in one redshift bin, where the bin size was $\Delta z = 0.005$.

To characterize each group, we estimate its line-of-sight velocity dispersion (σ_v) utilizing the ROSTAT package (Beers, Flynn, & Gebhardt 1990). This package avoids assumptions of gaussianity in the underlying velocity distributions and includes bootstrap and jackknife error estimation for the group redshifts and dispersions. Many of these estimators are significantly more resistant to non-gaussianity in the sample than the traditional Gaussian; large differences between the different scale measures can be a sign of deviations from gaussianity in the sample, either in shape or due to outliers. In particular, we use three estimators. The first, σ_{gap}, is based on the gapper algorithm, which is recommended for very small datasets (Beers et al. 1990). The error on this estimator is the jackknifed biweight estimate. The second is the biweight scale estimate, σ_{biwt}, which is recommended for datasets with ~ 10 members. Its confidence interval is taken from the jackknifed gapper. Finally, we use σ_{gauss}, the Gaussian estimator, and its 1-sigma Student's t error. Consistency among the various dispersion estimates for a small redshift sample lends credence to the measurement. However, we note that velocity dispersions based on a small number of redshifts can be highly uncertain (e.g., Zabludoff & Mulchaey 1998).

3.1. *The Group Associated with B1608+656*

The most prominent spike in the redshift distribution consists of eight galaxies with redshifts of $z \sim 0.63$. This spike includes the lensing galaxy at $z_\ell = 0.630$. However, we have not included the second lensing galaxy within the ring of images (G2; Koopmans et al. 2003; Surpi & Blandford 2003). All indications are that G2 is merging with G1, and therefore that this group consists of at least nine members. As one test of the likelihood that this redshift spike represents a real group, we have plotted the spatial distribution of the galaxies in the spike (Figure 2). We find that the galaxies are spatially concentrated and centered roughly on the position of the lens. Seven of the eight galaxies in the redshift spike, or eight out of nine if G2 is included, are within a circle centered on the lens system of radius 2.′1, corresponding to 1 h^{-1} comoving Mpc at the redshift of the lens. Figure 3 shows the redshift distribution in the region of the spike in terms of velocity offsets from the mean redshift of the group. The galaxies also have a tight distribution in velocity space, with all eight within ± 300 km s^{-1} of the mean redshift. Thus, we conclude that these galaxies represent a group, hereafter called Group 1, associated with the lensing galaxy.

For Group 1, we find that the various σ_v estimators obtained from the ROSTAT package are all consistent. This result strongly suggests that, despite the small number of redshifts in the group, the velocity distribution is well described by a Gaussian, and the resulting velocity dispersion is robust. In Table 1 we list the median redshift and the three estimates of the line-of-sight velocity dispersion (σ_{gap}, σ_{biwt}, and σ_{gauss}) with their associated errors (in km s^{-1}). Based on the number of group

[1] IRAF (Image Reduction and Analysis Facility) is distributed by the National Optical Astronomy Observatories, which are operated by the Association of Universities for Research in Astronomy under cooperative agreement with the National Science Foundation.

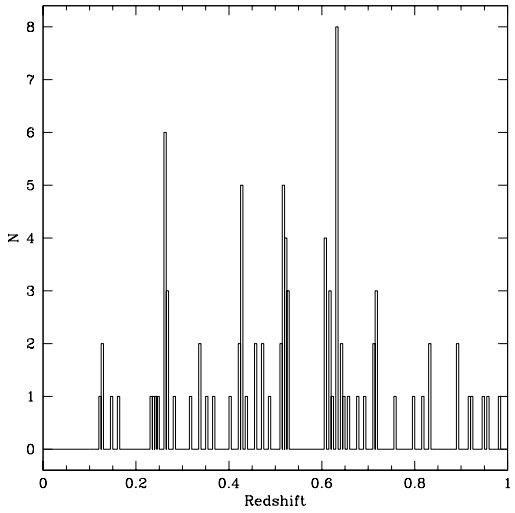

FIG. 1.— Histogram showing the distribution of the 97 non-stellar redshifts obtained in the field of B1608+656. The width of the bins is $\Delta z = 0.005$. The most prominent spike, with eight galaxies, is at the redshift of the lensing galaxy ($z = 0.63$).

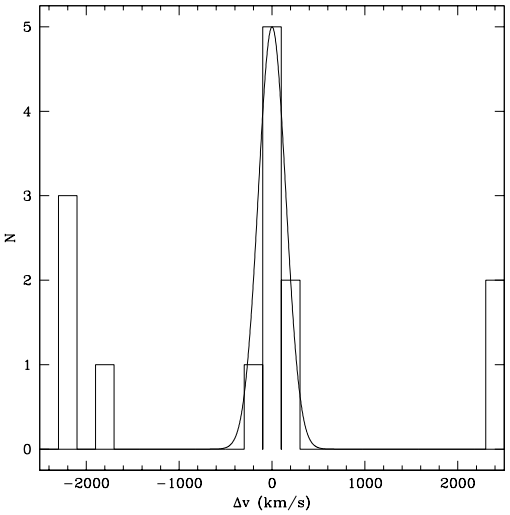

FIG. 3.— Histogram showing the velocity distribution of the galaxies in and surrounding the redshift spike at $z = 0.63$. The bin widths are 200 km s^{-1}, approximately twice the uncertainties in determining the redshifts. The curve is a Gaussian with σ =150 km s^{-1}.

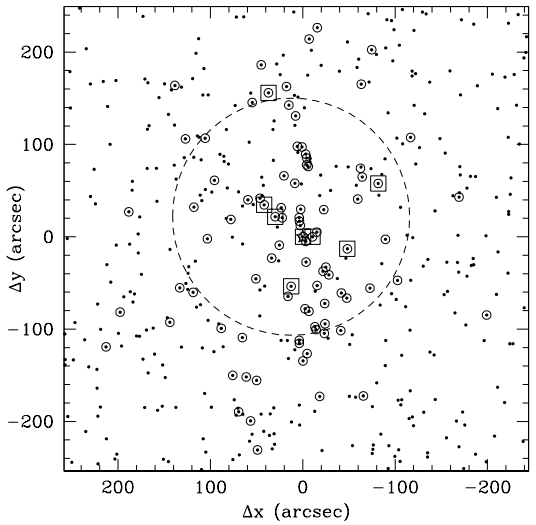

FIG. 2.— Spatial distribution of the galaxies in Group 1. The field of view is 10′x 11′, with the axes labeled in terms of offsets from the B1608+656 lens system in arcseconds. The dots represent the positions of galaxies with $r \leq 23$, while the open circles mark the galaxies for which redshifts have been obtained. The open boxes mark the galaxies in the group. The large dashed circle has a radius of 1 h^{-1} comoving Mpc at the redshift of the lensing galaxy.

members, we use $\sigma_v = \sigma_{gap}$ for Group 1, since σ_{gap} is the more appropriate estimator for very small data sets (Beers et al. 1990). Thus, we obtain $\sigma_v = 150 \pm 60$ km s^{-1}.

3.2. *Other Mass Concentrations Along the Line of Sight*

There are other spikes in the distribution of measured redshifts shown in Figure 1. In addition to the group at the redshift of the lens, there are three other group candidates in the observed distribution satisfying the redshift and spatial concentration criteria, with mean redshifts of $< z >= 0.265$ (Group 2), $< z >= 0.426$ (Group 3), and $< z >= 0.520$ (Group 4). Each group has a substantial number of confirmed members, with sizes of nine, seven, and 14 galaxies, respectively. The properties of these groups are given in Table 1. For each group, we find that the various σ_v estimators are all consistent. Based on the number of confirmed members in each group, we estimate the group velocity dispersions with σ_{gap} for Groups 2 and 3, and σ_{biwt} for Group 4. Figures 4 and 5 show the spatial and velocity distributions, respectively, for the three additional groups detected in this field. We explore the effects that these groups may have on the determination of H_0 from B1608+656 in the following sections.

4. DISCUSSION

4.1. *A Cluster at $z = 0.52$?*

Of the three additional candidate groups, the one at $z = 0.520$ stands out. Its velocity dispersion of ∼900 km s^{-1} implies that this structure is a cluster of galaxies rather than a group. If it is in fact a real cluster, it will have a significant effect on the measured value of H_0 obtained from the B1608+656 lens system (see next section). Therefore, we consider evidence that pertains to the reality of the cluster.

There are two main arguments in favor of the redshift spike's representing a real cluster. The first is the concentration of the structure in both velocity space and in projection on the sky. Nine of the 14 spectroscopically-confirmed galaxies in the structure are within ±1000km s^{-1} of the mean redshift, while 13 of 14 lie within a projected distance of 1 h^{-1} comoving Mpc of the median position. The second is that nine of the 14 galaxies in the group lie along a tight sequence on a color-magnitude diagram, at $(r - i) \sim 0.45$ (Figure 6).

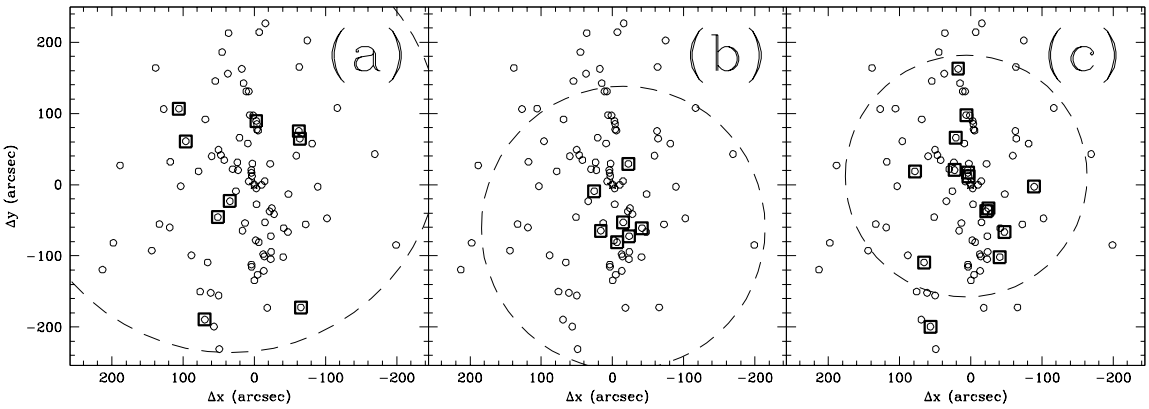

FIG. 4.— Spatial distributions of the galaxies in the additional three group candidates in the B1608+656 field, represented as in Figure 2. The open circles represent galaxies for which redshifts have been obtained, while the open boxes represent confirmed group members. The dashed circle in each plot has a radius of $1h^{-1}$ comoving Mpc at the redshift of the group and is centered at the median position of the confirmed group members. (a) Group 2 at $z \sim 0.27$. (b) Group 3 at $z \sim 0.43$. (c) Group 4 at $z \sim 0.52$.

TABLE 1
GROUP PROPERTIES

Group	$< z >$	$D_{\ell s}/D_s$	N_{gals}	σ_{gap} (km s^{-1})	σ_{biwt} (km s^{-1})	σ_{gauss} (km s^{-1})	θ_{med}[a] (arcsec)	PA$_{med}$[a] (°)	θ_{lw}[b] (arcsec)	PA$_{lw}$[b] (°)
1	0.6313	0.45	8[c]	150±60	130 ± 100	150^{+50}_{-20}	25	30	8	−5
2	0.2651	0.74	9	320±100	230 ± 270	320^{+120}_{-100}	69	29	18	6
3	0.4263	0.66	7	270±110	260 ± 120	270 ± 110	63	-166	46	−155
4	0.5202	0.53	14	920±120	930 ± 140	890^{+240}_{-130}	13	26	6	−47
4a[d]	0.5163	0.53	7	410±160	100±320	430±110	24	47	46	6
4b[d]	0.5241	0.53	7	360±120	350±120	350±120	44	−150	52	−161

[a]Median group position expressed as an offset from the lens. The PA is measured north through east.
[b]The luminosity-weighted group position expressed as an offset from the lens. The PA is measured north through east.
[c]This number does not include the second galaxy (G2) inside the Einstein ring of the lens system because there is no measured redshift for G2. However, G2 appears to be merging with the primary lens galaxy and thus appears to be a member of the group.
[d]Groups 4a and 4b are subsets of Group 4. See §4.1.

The arguments against the reality of the cluster are as follows. First, an examination of deep Advanced Camera for Surveys (ACS) images of this field (Program GO-10158; PI: Fassnacht) shows no obvious overdensity such as might be expected from a cluster. Furthermore, of the 11 galaxies that are members of Group 4 and also lie within the field of view of the ACS imaging, none appears to be a central bright early-type galaxy. In fact, nine out of the 11 group galaxies in the ACS imaging appear to be spirals. This is surprising given the red colors of these galaxies, but we will leave the discussion of this point to the followup paper in which we will focus on the properties of the groups and the galaxies within them. The second point arguing against the cluster hypothesis is that the group velocities (Figure 5c) are not normally distributed as one would expect from a relaxed cluster. With the large velocity dispersion implied by the measured redshifts, it is perhaps not unlikely that a random set of 14 galaxies does not produce a nice Gaussian shape. Further spectroscopy of the field, especially pushing deeper than the $r \sim 23$ limit used in the previous observations, may fill in the velocity structure and produce a velocity distribution that is closer to Gaussian. On the other hand, the last slitmask in our observing program had the targets re-prioritized to preferentially find galaxies in the cluster. Only one additional member was found, once again indicating that there is not the large overdensity of galaxies typically found in a cluster. Third, there was no extended X-ray emission detected in this field in a recent 30 ksec Chandra X-ray Observatory observation of this field (Dai & Kochanek 2005). If the cluster is as massive as suggested by its velocity dispersion and is virialized, it should have been detected by the Chandra observations, which had a 3-σ upper limit for detection that correspond to a velocity dispersion of $\sim$500 km s^{-1} (Dai & Kochanek 2005). However, it is possible that the cluster is recently formed or is, in fact, a pair of merging groups. In these situations, it may be severely underluminous at X-ray wavelengths. Finally, a cluster this massive and centered as close to the lens as it appears to be would introduce a strong effect on the lensing signature. The external shear introduced by such a cluster would be much larger than required by the lens model (Koopmans et al. 2003). Furthermore, it is possible that the surface mass density would be high enough at the position of the lens to form yet another image of the lensed source, i.e., the cluster would have to be treated in the strong lensing regime.

We feel that the arguments against the reality of the cluster are stronger than those in favor. The structure

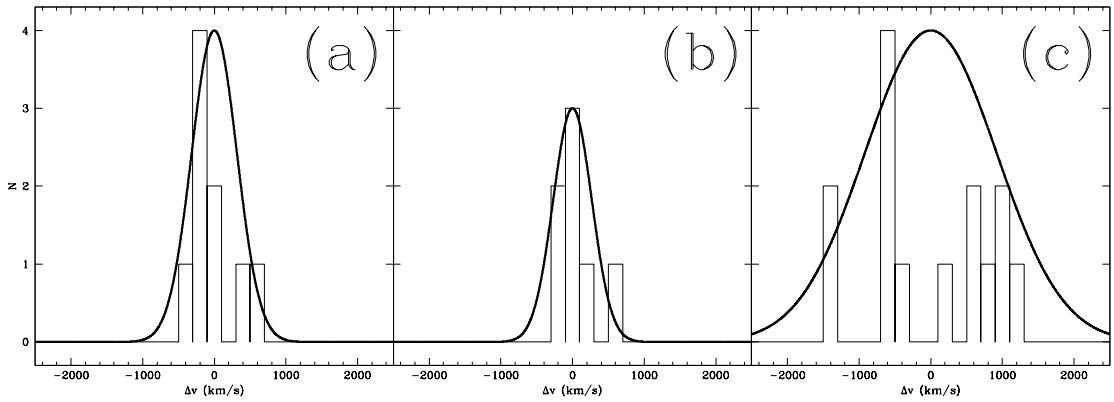

FIG. 5.— Histograms showing the velocity distributions of the galaxies in the three other spatially-concentrated redshift spikes. The bin widths are 200 km s^{-1}, approximately twice the uncertainties in determining the redshifts.

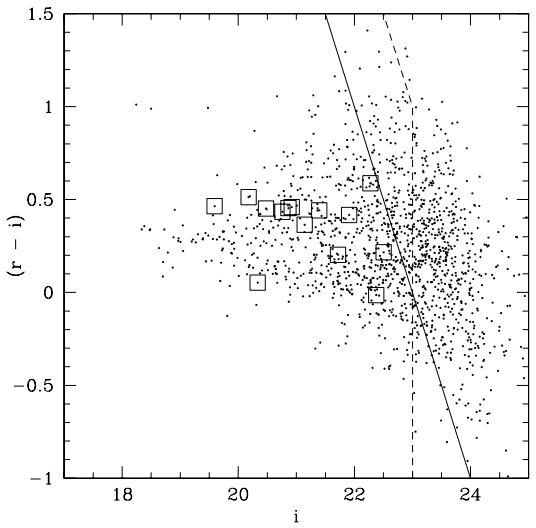

FIG. 6.— Color-magnitude diagram for the B1608+656 field. The dashed lines represent the approximate completeness limit of the imaging obtained at the Palomar 60-Inch Telescope. The boxed points belong to the $z = 0.52$ cluster candidate. The diagonal solid line represents the limit of the spectroscopy at $r \sim 23$.

may instead be a pair of merging groups or some kind of filamentary structure. To explore the two-group hypothesis, we arbitrarily split the group into two parts by redshift. Group 4a is defined as the seven galaxies with redshifts smaller than the median Group 4 redshift, while Group 4b is comprised of the seven galaxies with redshifts larger than the median. Figure 7 shows the spatial and velocity distributions of the two groups. The velocity dispersions of the two groups are ~ 400 km s^{-1} and ~ 350 km s^{-1}. If the two-group explanation is correct, and these velocity dispersions are close to the true values, then it is not surprising that the X-ray observations of Dai & Kochanek (2005) did not detect diffuse X-ray emission. The spatial distribution of Group 4b is centered slightly to the southwest of the Group 4a centroid. However, the two centroids are completely consistent, given the uncertainties. Another possibility is that the Group 4 galaxies lie along a filament. We note that much of the following discussion treats each group as a collection of individual halos, each associated with a group galaxy. Therefore, whether the galaxy under discussion is in a cluster, a group, or a filament is irrelevant.

4.2. *Effect on Gravitational Lensing*

We now consider the effect the groups associated with B1608+656 may have on the overall lensing gravitational potential, with a particular emphasis on the effect on H_0. While the angular separation of the lensed images in a gravitational lens system provides an accurate measurement of the projected lensing mass, it does not require that all of the mass be associated with the primary lensing galaxy. In fact, some of the mass can be contributed by other structures along the line of sight, such as the groups discussed above. The contribution of external mass is quantified through the convergence, κ_{ext}, that it causes at the location of the lensing galaxy. The convergence is just the scaled mass surface density:

$$\kappa_{ext} = \frac{\Sigma_{ext}}{\Sigma_c}; \quad \Sigma_c = \frac{c^2}{4\pi\, G}\frac{D_s}{D_\ell\, D_{\ell s}},$$

where Σ_c represents the critical mass surface density required for multiple images to form. As usual, D_ℓ, $D_{\ell s}$, and D_s are the angular diameter distances between observer and lens, lens and source, and observer and source, respectively. The external convergence will lead to a value of H_0 that is too high if the full lensing mass is improperly assigned solely to the primary lensing galaxy, i.e.,

$$H_{0,true} = H_{0,meas}(1 - \kappa_{ext}),$$

where $H_{0,meas}$ is the value obtained without properly including the external convergence in the lens model. We will use two methods to estimate the external convergence contributed by each of the groups along the line of sight to the B1608+656 system. Although neither of these methods may be entirely correct, the range of results that they produce should be representative of the true group convergences.

The first, and more traditional, method is to assume that the group can be approximated as a smooth mass distribution. The distribution, for simplicity, is usually taken to be that produced by a singular isothermal sphere (SIS). In this case, the convergence contributed

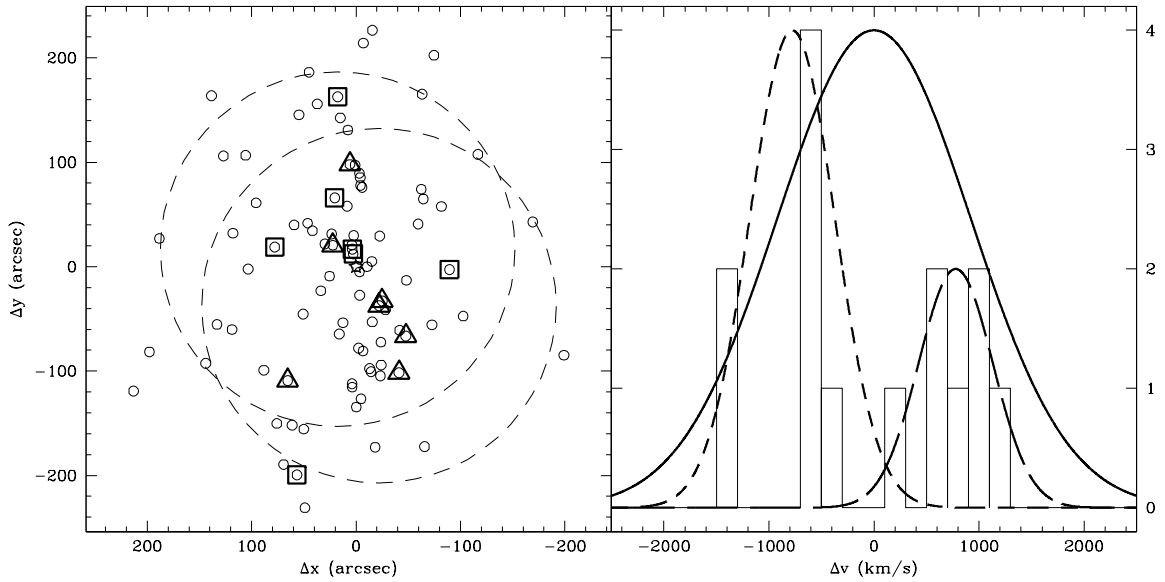

FIG. 7.— Spatial (left) and velocity (right) distributions of galaxies in Group 4. The galaxies have been split into two smaller groups in velocity space. The spatial distribution of Group 4a (redshifts smaller than the median Group 4 redshift) are marked by boxes. The galaxies in Group 4b are marked with triangles.

by the group, calculated at the location of the lens, is

$$\kappa_{SIS}(\theta_{cent}) = \frac{D_{\ell s}}{D_s}\frac{2\pi\sigma_v^2}{c^2\theta_{cent}} = \frac{b_{SIS}}{2\theta_{cent}},$$

where θ_{cent} is the angular offset between the center of the group and the lens system. The "lens strength" of an isothermal distribution is defined as $b = 4\pi\sigma_v^2 D_{\ell s}/(D_s c^2)$, and for a singular isothermal sphere gives the Einstein ring radius in angular units. If θ_{cent} is measured in arcminutes and σ_v is measured in km s^{-1}, then

$$\kappa_{SIS}(\theta_{cent}) \sim 0.015 \left(\frac{D_{\ell s}}{D_s}\right)\left(\frac{\sigma_v}{250\text{ km s}^{-1}}\right)^2\left(\frac{\theta_{cent}}{\text{arcmin}}\right)^{-1}.$$

The convergences due to the cluster and group candidates, calculated using the SIS assumption, are given in Table 2. In each case the velocity dispersion used was that obtained from the gapper method. With the strong dependence of κ_{ext} on θ_{cent}, it becomes imperative to locate the group centroid accurately, which is extremely difficult with fewer than several tens of confirmed group members. For example, the centroid estimates listed in Table 1 differ substantially depending on whether they were obtained by taking the median position or the luminosity-weighted position. Therefore, we also apply a second method for estimating the group convergence.

The alternate method for computing the group convergence is to treat the group as a collection of individual galaxy halos, with no overall group halo. In other words, the mass sheet at the position of the lensing galaxy is composed of the overlapping halos of the other galaxies in the group. The use of this method is motivated by two considerations. First, by ignoring any shared group halo, this method explores what is probably an extreme case, especially when assuming that the galaxy halos may be truncated (see below). This extreme case should provide a fairly robust lower limit to the estimate of the group convergence. Second, these moderate-redshift groups may still be in the early phases of formation and thus the galaxies may not yet have lost a significant fraction of their individual halos to the shared group halo. Simulations performed by Keeton & Zabludoff (2004) indicate that similar results are obtained whether the groups are treated as a single shared halo or a collection of individual halos. Furthermore, the input cosmological parameters (e.g., H_0) are recovered accurately when the group contribution is treated as a collection of galaxy halos. This accuracy is obtained even though they make the simplifying assumption that the group galaxies are circular when, in fact, their simulated galaxy mass distributions were elliptical. We follow the approach of Keeton & Zabludoff (2004) and assign group galaxy masses (expressed in terms of their lens strengths, b_i) based on their optical magnitudes (m_i) via the relationship

$$b_i = b_{fid}\ 10^{-0.2(m_i - m_{fid})},$$

where b_{fid} and m_{fid} are the lens strength and magnitude for a fiducial galaxy within the group. In each case, we take the fiducial galaxy to be the brightest confirmed group member. If each of the group members is treated as a singular isothermal sphere, as in Keeton & Zabludoff (2004), then the total convergence at the position of the lens is just the sum of the individual convergences at that position:

$$\kappa_{ind} = \sum_i \kappa_i = \sum_i \frac{b_i}{2\theta_i},$$

where θ_i is the distance between galaxy i and the lens. The results for each of the four groups are given in Table 2, while notes on the individual groups are given below.

Another effect to consider is that due to the truncation of the dark matter halos of the group galaxies. In the cal-

TABLE 2
Convergences due to Groups

Group	$\kappa_{SIS,med}$[a]	$\kappa_{SIS,lw}$[b]	κ_{ind}[c]	κ_{trunc}[c]	N_{trunc}[d]
1	0.0056	0.018	0.025	0.012	1
2	0.016	0.061	0.013–0.026	0.0040–0.0082	1
3	0.011	0.015	0.014–0.028	0.0064–0.013	2
4	···	···	0.026–0.053	0.015–0.031	3
4a	0.054	0.028	···	···	···
4b	0.023	0.019	···	···	···

[a]Convergence calculated with the group represented as a SIS and the group centroid represented by the median galaxy position.
[b]Convergence calculated with the group represented as a SIS and the group centroid represented by the luminosity-weighted mean.
[c]Range corresponds to a range of stellar velocity dispersions for the fiducial (brightest) galaxy in Groups 2, 3, and 4. The velocity dispersions range from 140–200 km s^{-1}.
[d]Number of galaxies contributing to κ_{trunc}.

culation of κ_{ind}, all of the galaxy halos are assumed to be larger than the separation between the galaxies and the primary lens system. However, weak lensing studies by Hoekstra, Yee, & Gladders (2004) have suggested that galaxy halos have a truncation radius of $\sim 200h^{-1}$ kpc. If this truncation radius is real and is typical, then the convergence due to galaxies located farther from the lens than this will drop off faster than the $(1/\theta)$ assumed in the calculation of κ_{ind}. To explore the possible size of this effect, we recalculate the external convergence contributed by each group, summing only the contributions from the galaxies that lie within a projected distance of $200h^{-1}$ comoving kpc from the lens. The results are given as κ_{trunc} in Table 2. This is an extreme approach, but it should give an approximate lower limit to the convergence caused by each group.

4.2.1. *Convergence Due to Group 1*

For this group we use F814W magnitudes measured from *Hubble Space Telescope* observations of the field. These observations consist of the deep ACS images mentioned above, as well as Wide-Field Planetary Camera 2 images of the same field (Program GO-6555: PI Schechter). The fiducial galaxy is the primary lensing galaxy (G1) which has a F814W magnitude of 18.2 and a lens strength of $b_{1608} = 0\farcs83$ (Koopmans et al. 2003). The group galaxy most distant from the lens system is not covered by the HST images so we do not include it in the calculation of κ_{ind}. However, it is far enough away ($2\farcm7$) that its contribution to the overall convergence is negligible.

4.2.2. *Convergence Due to Group 4*

As discussed in §4.1, we do not believe that Group 4 is a real cluster. We note that an assumption that the cluster is real yields extremely large convergences at the position of the B1608+656 system. The SIS approximation leads to $\kappa_{SIS} \sim 6.5/\theta$. For an isothermal sphere, another image of the background object will be produced when $\kappa > 0.5$. This condition is satisfied for the foreground cluster whether the cluster centroid is estimated using the luminosity-weighted position or the straight median position. Using these centroids leads to $\kappa = 1.1$ or $\kappa = 0.51$, respectively, at the position of the lens. We have not seen evidence for an obvious lensed counterpart in deep 5 GHz or 8.5 GHz radio maps, although there are other compact sources in the field (e.g., object 2; Fassnacht et al. 1999). Furthermore, such large convergences, whether from a SIS or some other mass distribution would almost certainly lead to an image separation in the main lens larger than the $2\farcs1$ that is observed. Once again, these arguments indicate that Group 4 is not a real cluster. Because the evidence against the reality of the cluster is strong, we instead apply the SIS approximation to our arbitrarily selected subgroups, 4a and 4b. For these groups, the convergences (Table 2) are much more reasonable

The calculation of κ_{ind} for Group 4 does not depend on whether the group is a single cluster or a pair of merging groups or a filament. For this group, the galaxy lens strengths are estimated from the r-band magnitudes from the ground-based imaging. The fiducial galaxy, which is the brightest confirmed group member, has $r = 20.0$. We will discuss different estimates of the lens strength of the fiducial galaxy below. We note here, however, that a galaxy at this redshift will have $b \sim 1$ if its stellar velocity dispersion is $\sim$260 km s^{-1}.

4.2.3. *Convergence Due to Groups 2 and 3*

The convergences calculated for Groups 2 and 3 using the SIS method are larger than that of Group 1 due to their larger velocity dispersions. For Group 3, the two SIS estimates of the convergences are similar because the group is compact and located approximately $1'$ from the lensing galaxy. In contrast, because Group 2 is roughly centered on the lens system, small displacements in the centroid can lead to large changes in κ_{SIS}. For both Group 2 and Group 3, the fiducial galaxies used in the κ_{ind} and κ_{trunc} methods are once again the brightest galaxies in their respective groups. In each case the fiducial galaxy has $r = 20.0$. Galaxies at the redshifts of Groups 2 and 3 have $b \sim 1$ for stellar velocity dispersions of $\sim$220 km s^{-1} and $\sim$230 km s^{-1}, respectively.

4.2.4. *Total Convergences of Groups 2, 3, and 4*

In order to compute the convergences for Groups 2–4, we need to assign a value for b_{fid} for each group. We do this by assuming that the fiducial galaxy in each

group has a velocity dispersion of 200 km s^{-1}. This is slightly smaller than the expected dark matter velocity dispersion for a L^* galaxy of $\sigma^*_{DM} \sim 225$ km s^{-1} (e.g., Kochanek 1996). Because the fiducial galaxy in each case is the brightest one in its respective group, this assumption should be reasonable. The resulting lens strengths are 0.85, 0.76, and 0.61 for Groups 2, 3, and 4, respectively. The resulting convergences are given as the upper end of the ranges given for κ_{ind} and κ_{trunc} in Table 2. These are within a factor of a few of the convergences estimated from assuming that the groups were isothermal spheres.

One factor that could lessen the total convergence arises from the conversion of the group galaxy luminosities to masses. For example, in the ACS images, several of the confirmed members of the groups appear to be late-type galaxies. In this case the estimated masses are probably too high since spirals have lower mass-to-light ratios than ellipticals (e.g., Bahcall, Lubin, & Dorman 1995). To explore this effect, we assume that the fiducial galaxy for Groups 2, 3, and 4 has a velocity dispersion of 140 km s^{-1}. The resulting lens strengths are ∼50% as large as those obtained above. The corresponding convergences are given as the lower ends of the ranges listed in the κ_{ind} and κ_{trunc} columns of Table 2.

In contrast, it is almost certain that not all of the group members have been identified. An incomplete census of the group will lead to an underestimate of the total convergence. We note that the deep ACS imaging of this field reveals at least 10 galaxies within 10″ of the lens, corresponding to $\sim 40 - 90\ h^{-1}$ comoving kpc at redshifts between 0.3 and 1.0. Only one of these galaxies has a measured redshift ($z = 0.6087$). Overall, a reasonable estimate is that true convergence from each group falls between the lower end of the κ_{trunc} range and the largest of the other estimates of κ_{ext}.

4.3. *Stellar Velocity Dispersion of the Lensing Galaxy*

Until now we have ignored another datum which can be used to break the mass-sheet degeneracy, namely the measured stellar velocity dispersion of the lensing galaxy. This measurement provides an estimate of the enclosed mass at a smaller radius than that probed by the lensing signature. Thus, the mass measurement from lensing can be combined with that from stellar dynamics to provide an effective mass density slope in the lensing galaxy (e.g., Koopmans & Treu 2002; Treu & Koopmans 2002). The result of adding an external mass sheet that is physically associated with the lensing galaxy is to flatten the overall mass density profile, which leads to a lower value of H_0 for given time delays. A measurement of the stellar velocity dispersion will reflect this flattening, i.e., the velocity dispersion will not be as high as would have been predicted from the lensing mass and an assumption of a steeper mass density profile. For a density profile that is close to isothermal (i.e., $\rho \propto r^{-2}$), essentially the same value of H_0 should be derived whether the system is modeled as a single galaxy with the effective mass density slope measured from lensing plus dynamics or as a galaxy with a steeper density profile but also including an external mass sheet (Koopmans 2004). For a high-accuracy measurement of H_0, it is thus crucial to obtain high precision measurements of either the external convergence or the stellar velocity dispersion of the lensing galaxy. In the case of B1608+656, the measured velocity dispersion is 247 ± 35 km s^{-1}, indicating that the mass distribution in the lens (including any contribution from the group) is close to isothermal (Koopmans et al. 2003). The uncertainties in the velocity dispersion are, in fact, the largest source of error in the current model.

4.4. *Effect of Large-scale Structure*

Finally, we consider the effect of the mass in large-scale structures (LSS) along the line of sight to the background source. In an ideal situation, it would be possible to account for all mass along the line of sight and to trace the rays from the background source through the distribution. In practice, even with deep space-based imaging, this is impractical. The uncertainties arising from photometric redshifts, the conversion of light to mass, etc., would far exceed the expected size of the effect. Therefore, it is necessary to examine the effect of LSS in a statistical manner. Analytic calculations have indicated that large-scale structure should affect the time delays for a lens system, and hence H_0, by a few percent (Seljak 1994) or perhaps as much as 10%, depending on the redshift of the background source (Bar-Kana 1996). The effect of LSS can be to either increase or decrease the value of H_0 because voids along the line of sight effectively act as areas of negative density when compared to the mean density of the Universe. Although this effect is a systematic one for any given lens system, it should be random for random lines of sight (e.g., Seljak 1994). Therefore, it should be possible to significantly reduce the uncertainty due to large-scale structures on the global measurement of H_0 by averaging the values obtained from many lens systems. We note that lenses may lie along lines of sight that are biased (e.g., have more line-of-sight structure) and therefore that the effect of large-scale structure can not be eliminated completely by averaging lens-based measurements of H_0. We will investigate this question in a future paper (Fassnacht et al., in prep).

4.4.1. *The Effect on H_0*

Finally, we arrive at the total effect on the value of H_0 derived from the B1608+656 system. The group physically associated with the lens system, Group 1, provides an external convergence of $\sim 0.01 - 0.03$ (Table 2). As discussed above, however, the degeneracy associated with Group 1 is broken by the measurement of the stellar velocity dispersion of the lensing galaxy. Therefore, the effect of Group 1 on the value of H_0 derived from this system gets folded into the determination of the radial mass slope in the lensing galaxy, and is thus already included in the published uncertainties on H_0 from B1608+656.

The other groups along the line of sight also provide convergences of a few percent. These groups are almost certainly typical of the clumpy structure that can be found along any line of sight. None of them provide an extraordinarily large convergence, unless Group 4 is a real cluster. Therefore, one would be inclined to incorporate the effects of these groups into the effects of LSS and conclude that these groups will contribute to the random shift of a few percent in the value of H_0 determined from this system. However, as a result of our investigation of lens fields (Fassnacht et al., in prep) we have determined that the B1608+656 system lies along

a line of sight that is overdense compared to typical lines of sight. Therefore, the expected effect of properly incorporating the effects of LSS on this system is to *reduce* the value of H_0 from the previously measured value. If the majority of the extra mass along this line of sight is being contributed by Groups 1-3, the size of the effect could be 5% or more, given the convergences in Table 2. This effect, thus, could be comparable in size to the statistical uncertainties quoted for the H_0 measurement from this system, and would reduce the central value to ∼70 km s^{-1} Mpc^{-1} or lower.

5. SUMMARY AND FUTURE WORK

Our spectroscopic observations of the field containing the lens system B1608+656 have provided evidence for four groups of galaxies along the line of sight to the lens system. These groups should contribute external convergence at the location of the lens and, therefore, will affect the determination of the Hubble Constant obtained with this system. However, quantifying the amount of external convergence is difficult. If each group contains all of its mass in a overall smooth halo, it becomes imperative to measure accurately the halo mass and centroid. These measurements can be highly uncertain when made based on ∼ 10 redshifts. We therefore follow a second approach and treat each group as a collection of individual galaxy halos. To establish a firm lower limit to the convergence due to each group, we examine the convergence contributed only by galaxies within a projected distance of 200 h^{-1} comoving kpc from the lens. However, our calculations do not include contributions from other galaxies within the truncation radius of the lens because their redshifts are unknown. Each of the groups contributes a convergence of a few percent. The overall effect on H_0 is less than suggested by the sum of the convergences because the stellar velocity dispersion of the main lensing galaxy has been measured. This measurement breaks the mass-sheet degeneracy, at least due to Group 1, by determining the effective radial mass density slope in the lensing galaxy. The effects of the other groups can be folded into the overall uncertainties due to large-scale structure along the line of sight, since none of the groups appears to be extremely massive. However, because the line of sight to B1608+656 appears to be significantly overdense compared to typical lines of sight, the effect of LSS will be to bias the current measurement of H_0 high, i.e., the true value of H_0 from this system should be lower than the published value. The size of the effect of the LSS could be 5% or larger. We note that none of the newly discovered groups was obvious from optical images of this system. Therefore, it is important to closely investigate the fields of lens systems in order to examine possible sources of bias in lens-based measurements of H_0, especially if the stellar velocity dispersion of the lensing galaxy is unknown.

We are actively working to reduce the uncertainties in the determination of H_0 from this lens system. The deep ACS imaging is being used as an input to new lensing code that can properly incorporate Einstein ring structure. This modeling should reduce the mass-slope uncertainties substantially in the region of the lensed images. We will also use the ACS imaging to search for weak lensing signatures of mass concentrations along the line of sight to the lens system. The weak lensing will provide further constraints on the amount of external convergence for B1608+656. Another approach to reducing the uncertainties in the mass slope would be to obtain higher sensitivity spectroscopy of the lensing galaxy. The spectroscopy would provide a more accurate determination of the stellar velocity dispersion. Further optical spectroscopy of the galaxies in the field and deeper X-ray imaging would also add information on the external mass distribution. Finally, by averaging measurements of H_0 obtained from many different lens systems, we should be able to reduce the uncertainties due to large-scale structure and thus obtain a precise global measurement of H_0 from lensing.

We thank Leon Koopmans, Tommaso Treu, and Tony Tyson for useful discussions. We thank the anonymous referee for his or her comments. CDF and JPM acknowledge support under HST program #GO-10158. Support for program #GO-10158 was provided by NASA through a grant from the Space Telescope Science Institute, which is operated by the Association of Universities for Research in Astronomy, Inc., under NASA contract NAS 5-26555. These observations would not have been possible without the expertise and dedication of the staffs of the Palomar and Keck observatories. We especially thank Paola Amico, Karl Dunscombe, Grant Hill, Jean Mueller, Ron Quick, Kevin Rykoski, Gabrelle Saurage, Chuck Sorenson, Skip Staples, Wayne Wack, Cindy Wilburn, and Greg Wirth. Some of the data presented herein were obtained at the W. M. Keck Observatory, which is operated as a scientific partnership among the California Institute of Technology, the University of California and the National Aeronautics and Space Administration. The Observatory was made possible by the generous financial support of the W.M. Keck Foundation. The authors wish to recognize and acknowledge the very significant cultural role and reverence that the summit of Mauna Kea has always had within the indigenous Hawaiian community. We are most fortunate to have the opportunity to conduct observations from this mountain. This work is supported in part by the European Community's Sixth Framework Marie Curie Research Training Network Programme, Contract No. MRTN-CT-2004-505183 'ANGLES'.

REFERENCES

Bahcall, N. A., Lubin, L. M., & Dorman, V. 1995, ApJ, 447, L81.
Bar-Kana, R. 1996, ApJ,468, 17
Beers, T. C., Flynn, K., & Gebhardt, K. 1990, AJ, 100, 32
Cohn, J. D., Kochanek, C. S., McLeod, B. A., & Keeton, C. R. 2001, ApJ, 554, 1216
Dai, X. & Kochanek, C. S. 2005, ApJ, 625, 633
Falco, E. E., Gorenstein, M. V., & Shapiro, I. I. 1985, ApJ, 289, L1
Fassnacht, C. D., Womble D. S., Neugebauer, G., Browne, I. W. A., Readhead, A. C. S., Matthews, K., & Pearson, T. J. 1996, ApJ, 460, L103
Fassnacht, C. D., Pearson, T. J., Readhead, A. C. S., Browne, I. W. A., Koopmans, L. V. E., Myers, S. T., & Wilkinson, P. N. 1999, ApJ, 527, 498
Fassnacht, C. D. & Lubin, L. M. 2002, AJ, 123, 627

Fassnacht, C. D., Xanthopoulos, E., Koopmans, L. V. E., & Rusin, D. 2002, ApJ, 581, 823
Hoekstra, H., Yee, H. K. C., & Gladders, M. D. 2004, ApJ, 606, 67
Keeton, C. R., & Zabludoff, A. I. 2004, ApJ, 612, 660
Kochanek, C. S. 1996, ApJ, 466,638
Kochanek, C. S., Keeton, C. R., & McLeod, B. M. 2001, ApJ, 547, 50
Koopmans, L. V. E. 2004, in *Baryons in Dark Matter Halos*, R. Dettmar, U. Klein, P. Salucci, eds., 66.1
Koopmans, L. V. E., & Treu, T. 2002, ApJ, 568, L5
Koopmans, L. V. E., Treu, T., Fassnacht, C. D., Blandford, R. D., & Surpi, G. 2003, ApJ, 599, 70
Myers, S. T., et al. 1995, ApJ, 447, L5
Oguri, M., et al. 2004, ApJ, 605, 78
Oke, J. B., et al. 1995, PASP, 107, 375
Refsdal, S. 1964, MNRAS, 128, 307
Rusin, D., Norbury, M., Biggs, A. D., Marlow, D. R., Jackson, N. J., Browne, I. W. A., Wilkinson, P. N., & Myers, S. T. 2002, MNRAS, 330, 205
Seljak, U. 1994, ApJ, 436, 509
Sheinis, A. I., Bolte, M., Epps, H. W., Kibrick, R. I., Miller, J. S., Radovan, M. V., Bigelow, B. C., & Sutin, B. M. 2002, PASP, 114, 851
Surpi, G., & Blandford, R. D. 2003, ApJ, 584, 100
Thuan, T. X. & Gunn, J. E. 1976, PASP, 88, 543
Treu, T., & Koopmans, L. V. E. 2002, MNRAS, 337, L6
Treu, T., & Koopmans, L. V. E. 2004, ApJ, 611, 739
Walsh, D., Carswell, R. F., & Weymann, R. J. 1979, Nature, 279, 381
Wilman, D. J., Balogh, M. L., Bower, R. G., Mulchaey J. S., Oemler Jr., A., Carlberg, R. G., Morris, S. L., & Whitaker, R. J. 2005, MNRAS, 358, 71
Zabludoff, A. I. & Mulchaey, J. S. 1998, ApJ, 496, 39